Heat Transfer in Laminar and Turbulent Flows Between Parallel Plates with Transverse Flow

SHAW MEI LEE and WILLIAM N. GILL

Syracuse University, Syracuse, New York

An interesting aspect of convective heat transfer is transpiration cooling, where in the simplest case the wall is made of a porous material to allow the injection or suction of fluid through it. This effective method for cooling is especially important in protecting walls when heat transfer is intense, such as in combustion chamber walls and exhaust nozzles. Furthermore, it seems probable that porous walled flow reactors, which employ secondary transverse flows, will be used for a variety of applications in the future. Such reactors offer attractive features regarding the control of concentration and temperature distributions.

Experimental investigation of flow over flat plates with suction or injection was carried out by Mickley et al. (5). Eckert et al. (*1*) investigated the roughness effect of the wall on the velocity profile for turbulent flow in a channel with a porous lower wall, but heat transfer was not considered. Yuan and Finkelstein (*7*) analytically studied heat transfer in laminar conduit flow with coolant injection, and Yuan (*6, 8*) later analyzed turbulent heat transfer in a channel with suction or injection by assuming the axial velocity and the rate of injection and suction varied as an exponential function of axial distance.

A simplified model of transpiration cooling in turbulent systems was adopted for the present investigation, wherein the secondary flow velocity is uniform. This is perhaps the simplest problem involving transverse flow with a turbulent main stream that one can consider, but it retains many of the essential features of more complicated systems and thereby provides useful design information regarding both conduit and boundary-layer flows. Since no reliable experimental information is available, the mixing length used in previous studies (*3, 4*) was assumed to be applicable here also. It is believed that the results will qualitatively describe heat transfer in the turbulent region, and this is confirmed, partially at least, by the agreement between the correlation of present analytical results and the correlation obtained by Mickley et al. (5) of their turbulent boundary-layer measurements.

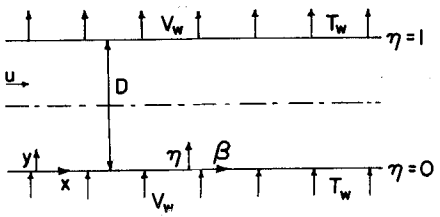

Fig. 1. Coordinate system.

In reference *4* the mixing length expression used for the present study was employed to investigate heat transfer in the laminar-turbulent region, and it was pointed out that the Reynolds number at which transition takes place is uncertain since it depends on many factors. However, the velocity distributions obtained agreed rather well with experimental data (*3*) in the transition region, and the heat transfer results were qualitatively correct, which is believed to be the case for the present results as well. As before, the transition point in this study is $N_{Re} = 4{,}800$, and curves marked with that value are for laminar flow. Roughly, the transition region here is for Reynolds numbers from 4,800 to about 15,000.

ANALYSIS

The coordinates used are shown in Figure 1, and the rates of fluid injection at the lower wall and suction at the upper wall are taken to be the same and constant. Fluid used for injection is the same as the fluid flowing in the channel, and constant fluid properties are assumed. Flow is fully developed, and the temperature distribution is linear and can be expressed by

$$T - T_o = A_t \xi + \phi(\eta) \tag{1}$$

so that

$$T_w - T_o = A_t \xi + \phi(0)$$

and

$$\theta = \frac{T - T_w}{A_t}$$

The momentum equation in dimensionless form is

$$U\frac{\partial U}{\partial \beta} + V\frac{\partial U}{\partial \eta} = -\frac{\partial P}{\partial \beta} + \frac{1}{N_{Re_o}}\frac{\partial^2 U}{\partial \eta^2} + \frac{\partial}{\partial \eta}\left(L_m^2 \left| \frac{\partial U}{\partial \eta} \right| \frac{\partial U}{\partial \eta} \right) \tag{2}$$

where L_m is assumed to be symmetrical about $\eta = \frac{1}{2}$ and is given by

$$L_m = 0.36\eta\,(1 - e^{-\phi\eta}); \quad \phi = \frac{y_m{}^+ - 60}{11}; \quad \eta \leq 1/2$$

Also, the continuity equation is

$$\frac{\partial U}{\partial \beta} + \frac{\partial V}{\partial \eta} = 0$$

For fully developed flow, $\partial U/\partial \beta = 0$; then $\partial V/\partial \eta = 0$, and the transverse velocity $V = V_w$ is constant. Pressure

becomes a function of β only, and the pressure gradient is a constant so that

$$-\frac{dP}{d\beta} = C_1 \tag{3}$$

If one integrates the momentum equation and then rearranges it, the result is

$$\frac{dU}{d\eta} = \frac{V_w U - (C_1 \eta + C_2)}{\left(\frac{1}{N_{Re_o}} + L_m^2 \left| \frac{dU}{d\eta} \right|\right)} \tag{4}$$

When one uses the conditions of no slip at the walls, $U(0) = U(1) = 0$, the following expressions are obtained for C_1 and C_2:

$$C_1 = \frac{1}{N_{Re_o}} \left[\left(\frac{dU}{d\eta}\right)_o - \left(\frac{dU}{d\eta}\right)_1 \right] \tag{5a}$$

$$C_2 = \frac{-1}{N_{Re_o}} \left(\frac{dU}{d\eta}\right)_o \tag{5b}$$

Since analytical solution of Equation (4) is inconvenient, an iteration method is used to solve for the velocity distribution. Integration of Equation (4) twice gives two equations, and with the following conditions

$$U(0) = U(1) = 0 \tag{6a}$$

$$\int_o^1 U d\eta = 1 \tag{6b}$$

these equations can be used to solve for the constants C_1 and C_2 as

$$C_1 = \frac{V_w S_1 S_6 - S_3 (S_4 V_w - 1)}{S_2 S_6 - S_3 S_5} \tag{7a}$$

$$C_2 = \frac{S_2 (S_4 V_w - 1) - S_1 S_5 V_w}{S_2 S_6 - S_3 S_5} \tag{7b}$$

where the $S_j (j = 1, 2, \ldots, 6)$ are given in the Appendix.

The energy equation in dimensionless form is

$$U \frac{\partial T^*}{\partial \beta} + V_w \frac{\partial T^*}{d\eta} = \frac{\partial}{\partial \eta} \left(\frac{1}{N_{Re_o}} + L_h^2 \left| \frac{dU}{d\eta} \right| \right) \frac{\partial T^*}{\partial \eta} \tag{8}$$

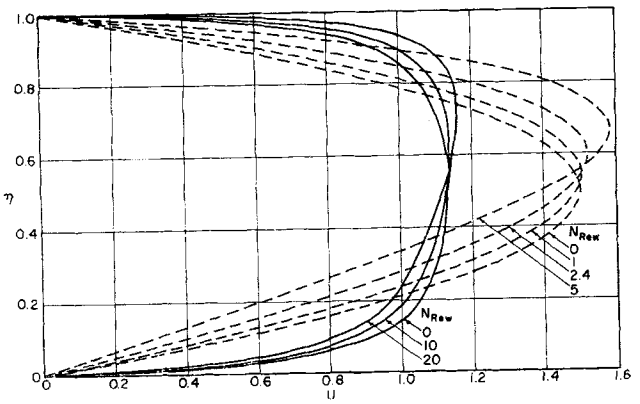

Fig. 2. Effect of blowing on velocity profiles. Solid lines represent $N_{Re} = 12, 120$, and dashed lines represent laminar flow.

This equation can be reduced easily to a Sturm-Liouville system, but here only the asymptotic fully developed solution will be determined. The entrance region problem and also the case of nonlinear flow are being investigated currently and will be reported at a later date.

When one applies the linear temperature expression and the dimensionless temperature θ, the energy equation becomes

$$U + N_{Pe_o} V_w \frac{d\theta}{d\eta} = \frac{d}{d\eta} \left[\left(1 + N_{Pe_o} L_h^2 \left| \frac{dU}{d\eta} \right| \right) \frac{d\theta}{d\eta} \right] \tag{9}$$

and

$$\theta(1) = \theta(0) = 0 \tag{10}$$

Integration of Equation (9) yields

$$\frac{d\theta}{d\eta} = \frac{1}{F(\eta)} \left[\int_o^\eta U d\eta + N_{Pe_o} V_w \theta + \left(\frac{d\theta}{d\eta}\right)_o \right] \tag{11}$$

where

$$F(\eta) = \left(1 + N_{Pe_o} L_h^2 \left| \frac{dU}{d\eta} \right| \right)$$

Then from the boundary conditions, the temperature gradients at both walls are related by

$$\left(\frac{d\theta}{d\eta}\right)_1 = \left(\frac{d\theta}{d\eta}\right)_o + 1 \tag{12}$$

and the solution to Equation (11) is

$$\theta = e^{V_w N_{Pe_o} \int_o^\eta \frac{d\eta}{F(\eta)}} \left\{ \int_o^\eta \left[\frac{\left(\int_o^\eta U d\eta \right) \left(e^{-V_w N_{Pe_o} \int_o^\eta \frac{d\eta}{F(\eta)}} \right)}{F(\eta)} \right] d\eta + \left(\frac{d\theta}{d\eta}\right)_o \int_o^\eta \frac{e^{-V_w N_{Pe_o} \int_o^\eta \frac{d\eta}{F(\eta)}}}{F(\eta)} d\eta \right\} \tag{13}$$

where

$$\left(\frac{d\theta}{d\eta}\right)_o = \frac{\int_o^1 \left[\frac{\left(\int_o^\eta U d\eta \right) \left(e^{-V_w N_{Pe_o} \int_o^\eta \frac{d\eta}{F(\eta)}} \right)}{F(\eta)} \right] d\eta}{\int_o^1 \frac{e^{-V_w N_{Pe_o} \int_o^\eta \frac{d\eta}{F(\eta)}}}{F(\eta)} d\eta} \tag{14}$$

With the expressions given above, one can determine the velocity and temperature profiles. For this purpose the mixing length expression given previously (3, 4) was used, and the turbulent Prandtl number is taken as unity.

Results for laminar flow can easily be checked with the analytical solution. To do this, Equation (4) is solved, and the velocity distribution is found to be

$$U = \frac{2N_{Rew} \left[1 + (e^{N_{Rew}} - 1)\eta - e^{\eta N_{Rew}} \right]}{(N_{Rew} + 2) + e^{N_{Rew}} (N_{Rew} - 2)} \tag{15}$$

where the wall Reynolds number N_{Rew} is defined as

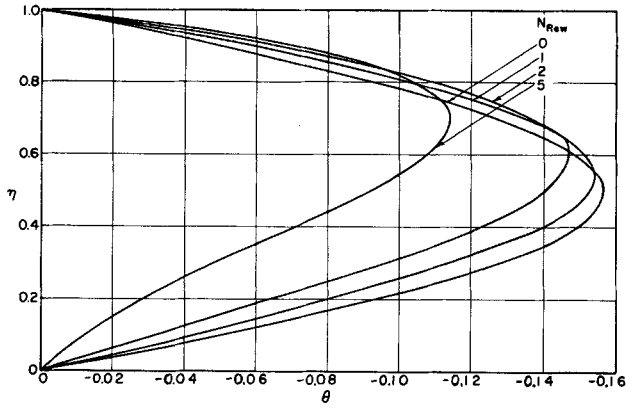

Fig. 3a. Effect of blowing on laminar temperature profiles, $N_{Pr} = 1$.

$$N_{Rew} = \frac{Dv_w}{\nu}$$

Equation (15) was then substituted into Equation (9), and the solution of the energy equation was found to be

$$\theta = \frac{2}{Q_8}\left[\eta Q_2 - \eta^2 Q_4 + Q_3 - Q_5\, e^{N_{Rew}\eta} + Q_1\, e^{N_{Rew}N_{Pr}\eta}\right] - \frac{\left(\frac{d\theta}{d\eta}\right)_o}{N_{Rew}N_{Pr}}\left(1 - e^{N_{Rew}N_{Pr}\eta}\right) \quad (16)$$

$$\left(\frac{d\theta}{d\eta}\right)_o = \frac{2N_{Rew}N_{Pr}}{(e^{-N_{Rew}N_{Pr}} - 1)Q_6}\left[e^{-N_{Rew}N_{Pr}}(Q_2 - Q_4 + Q_3) - Q_5\, e^{N_{Rew}(1-N_{Pr})} + Q_1\right] \quad (17)$$

θ_b, Q_n $(n = 1, \ldots, 6)$ are given in the Appendix.

These equations are used for checking the results of the laminar flow case, but the expression for θ_b is not particularly convenient for computation when N_{Pr} and N_{Rew} are large; for example $N_{Pr} \geqq 10$ and $N_{Rew} \geqq 1$.

For the lower wall, N_{Nu} and the Fanning friction factor F are given by

$$N_{Nu_l} = \frac{2h_l D}{k} = \frac{2\left(\frac{d\theta}{d\eta}\right)_l}{\theta_b} \quad (18)$$

and

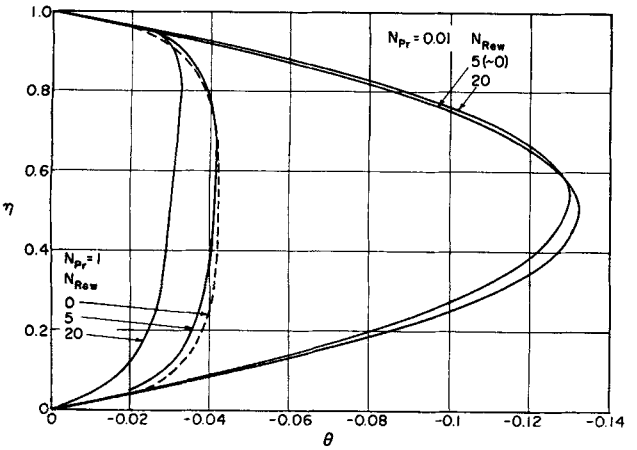

Fig. 3b. Effect of blowing on turbulent temperature profiles, $N_{Re} = 7{,}688$, $N_{Pr} = 0.01, 1$.

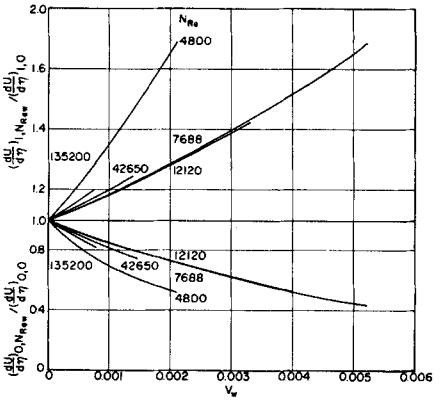

Fig. 4. Effects of blowing and turbulence on wall velocity gradients, $N_{Pr} = 1$.

$$F_l = \frac{2}{N_{Re_o}} \frac{\left(\frac{dU}{d\eta}\right)_l}{U_b} \quad (19)$$

where the wall heat flux is

$$q_l = h_l\,(T_w - T_b) = -k\left(\frac{dT}{dy}\right)_l$$

and the average temperature is defined by

$$\theta_b = \int_o^1 U\theta\, d\eta \quad (20)$$

RESULTS AND DISCUSSION

Results are presented in Figures 2 to 7, and numerical data on Nusselt numbers for various values of the parameters are given elsewhere.* Figures 2 and 3 indicate that velocity and temperature profiles become more skewed with increased rate of cross flow, and Figures 3 show that for fluids with small N_{Pr} the effect of cross flow on temperature profiles is rather small, while for fluids with large N_{Pr} this effect is pronounced. This occurs because the contribution of transverse convection is less important when fluids with high molecular conductivity are involved.

As expected, the friction factor and N_{Nu} decrease with injection and increase with suction. Figures 4 and 5 show the combined effect of cross-flow rate and turbulence on velocity and temperature gradients at the wall. The curves indicate that for constant N_{Re}, temperature and velocity gradients at the walls decrease with increasing rate of fluid injection and increase with increasing rate of fluid suction. For a constant dimensionless cross-flow rate V_w,

* Tabular material has been deposited as document 8087 with the American Documentation Institute, Photoduplication Service, Library of Congress, Washington 25, D. C., and may be obtained for $1.25 for photoprints or 35-mm. microfilm.

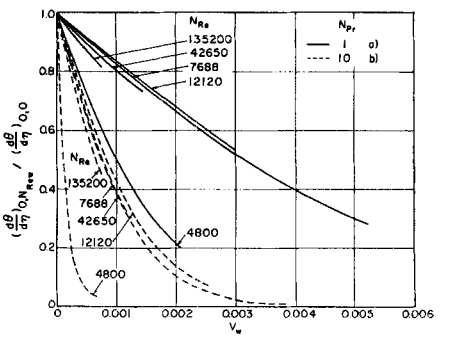

Fig. 5. Effects of blowing and turbulence on wall temperature gradient.

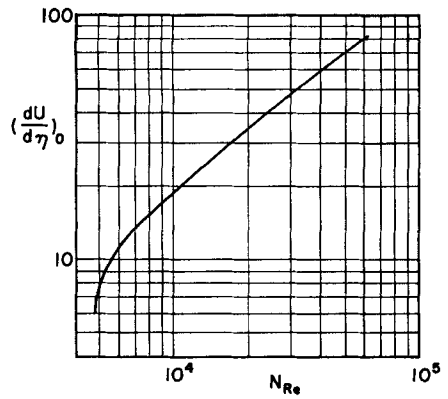

Fig. 6. The variation of wall velocity gradient with respect to Reynolds number.

as N_{Re} increases, the effect of cross flow on the gradients decreases first and then increases when N_{Re} becomes sufficiently high. This is due to the interplay of turbulence and the effect of injection and suction of fluid on the wall layer.

At the lower wall, injection tends to decrease the wall velocity gradient, and at the upper wall suction tends to increase it, whereas turbulence flattens the velocity profile and makes both wall velocity gradients larger. From the calculation of velocity profiles for various N_{Re} with no blowing, the increase of the wall velocity gradient is known to be much greater in the transition region than in the high N_{Re} region as shown in Figure 6. Therefore, in the low N_{Re} region, the effect of turbulence on wall velocity gradients is more important than that due to suction and injection. At the upper wall, the effects of suction and turbulence on wall velocity gradients complement each other, while at the lower wall the reverse is true. Therefore, in the lower N_{Re} region, the effect of N_{Re} counteracts the influence of V_w on the wall velocity gradient, but when N_{Re} is sufficiently high, the decrease in the thickness of the wall layer is small compared with the increase in N_{Re}; thus the effects due to injection and suction become dominant, and as a result the role of N_{Re} is to increase the importance of V_w on the wall velocity gradient. However, the N_{Re} effect in this region is small compared with that in low N_{Re} region.

An alternate description is that turbulent diffusion diminishes the effect of cross-flow convection, but the intensity of turbulence increases more slowly than the increase in transverse convection which occurs when N_{Re} increases for a given V_w, fluid, and conduit. That is, initially turbulent diffusion increases rapidly (say just above the laminar region), but as N_{Re} continues to increase, turbulent diffusion is offset by transverse convection.

In Figure 4 the ordinate also expresses the ratio of friction factor with blowing to that without blowing. The average value of this ratio for the upper and lower walls increases with increasing cross-flow rate.

Figure 5 shows the effect of blowing on wall temperature gradients for fluids of $N_{Pr} = 1$ and 10. For fluids with high N_{Pr} the wall temperature gradient is greatly affected by cross flow. The effects of N_{Re} and V_w are very much like that of Figure 4 and were already discussed in previous paragraphs.

The Nusselt numbers are tabulated elsewhere* for various N_{Re} and N_{Pr}. Examination of these data shows that N_{Nu} increases with suction and decreases with injection of fluid. For fluids with low N_{Pr} the effect of cross flow on N_{Nu} is very small, while for fluids with high N_{Pr} this effect is prominent. This may be due to the difference in laminar wall-layer thickness. Since for high N_{Pr} fluids the main resistance to heat transfer is caused by this layer, disturbances in this layer naturally will show a large effect. The average N_{Nu} of lower and upper walls increases slightly with increasing cross-flow rate.

One interesting aspect of the present study is the application of the present results to turbulent boundary-layer flow over a flat plate with suction or injection of fluid. Mickley et al. (5) analyzed the boundary-layer flow by film theory and obtained in terms of the ratio of the heat transfer coefficients with blowing, h, to that without blowing, h_o

$$\frac{h}{h_o} = \frac{\phi'}{e^{\phi'} - 1} \tag{22}$$

where

$$\phi' = \frac{V_w}{u_s}\frac{1}{N_{sto}} = \frac{\rho V_w C_p}{h_o}$$

and u_s is the main stream velocity. This equation is in the same form as that derived for the laminar Couette flow with a constant rate of injection and suction at the walls (2). For the latter case, the parameter ϕ' is defined to be

$$\phi' = N_{Rew} N_{Pr}$$

Experimental data of Mickley et al. for turbulent boundary-layer flow over a flat plate with injection or suction of fluid were correlated by Equation (22). The data show some scatter on both sides of the curves.

Results of the present analysis were correlated in Figures 7 for the cases of $N_{Pr} = 1$ and 10. The points represent computed values and the solid curves represent the following equation:

$$\frac{h}{h_o} = \frac{N_{Rew} N_{Pr}}{(e^{N_{Rew}N_{Pr}} - 1)} \tag{23}$$

$V_w \frac{1}{N_{sto}}$ was used as the abscissa. The figure shows that except for $N_{Re} = 4{,}800$ the computed h/h_o for both N_{Pr} can be represented closely by Equation (22). For injection the equation defines the upper limit, while for suction it defines the lower limit. Since velocity profiles are not symmetric and displacements are most pronounced in the laminar case, the results were corrected by multiplying

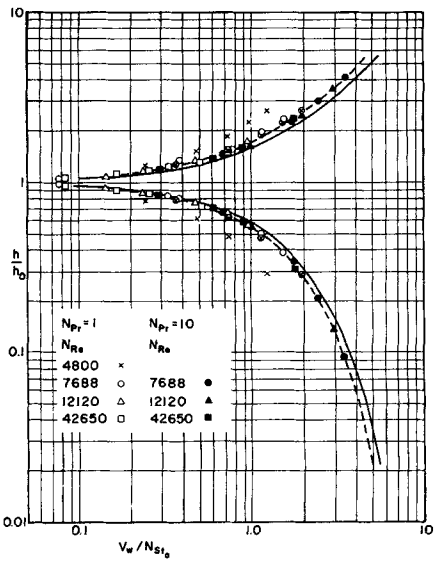

Fig. 7. Ratio of heat transfer coefficients with and without blowing vs. V_w/N_{St_o}, $N_{Pr} = 1$, 10. Times sign in a circle represents the laminar case $N_{Pr} = 1$ and $N_{Re} = 4{,}800$ with the abscissa multiplied by U_m.

* See footnote on p. 898.

the abscissa by U_m. This correction as shown on Figure 7 is reasonably good.

Since heat transfer coefficients for the no blowing case, h_o, have been well established, the following correlation equation can be used to estimate the heat transfer coefficients for turbulent forced convection with transverse flow in conduits:

$$\frac{h}{h_o} = \frac{\alpha\phi'}{e^{\alpha\phi'} - 1} \tag{24}$$

where

$$\alpha = \frac{1}{1.1} \text{ for injection}$$

$$\alpha = \frac{1}{1.2} \text{ for suction}$$

This is a remarkably simple result which should provide reasonable estimates for design purposes.

NOTATION

A, A_t = axial temperature gradients, $AN_{Peo} = A_t$
D = distance between the plates
F = Fanning friction factor
h = heat transfer coefficient
h_o = heat transfer coefficient with no transverse flow
L_h, L_m = dimensionless mixing length of heat and momentum, that is mixing length divided by D
P = dimensionless pressure, $p/\rho u_b^2$
q = heat flux
T = temperature
T_o = reference temperature
T^* = dimensionless temperature, T/A_t
u, v = axial and transverse velocities
u^* = friction velocity
U = dimensionless axial velocity, u/u_b
V = dimensionless transverse velocity, v/u_b
x, y = axial distance and transverse distance from wall
y_m^+ = dimensionless transverse distance, $(D\,u^*)/2\nu$

Greek Letters

β = dimensionless axial distance, x/D
η = dimensionless distance from the lower wall, y/D
θ = dimensionless temperature, $[\phi(\eta) - \phi(0)]/A_t = T^* - T^*_w$
μ = viscosity
ν = kinematic viscosity
ξ = x/DN_{Peo}
ρ = density
ϕ = temperature function defined by Equation (1)

Dimensionless Groups

N_{Nu} = Nusselt number, $2hD/k$
N_{Pe} = Peclet number, $N_{Re}N_{Pr}$
N_{Peo} = $N_{Reo}N_{Pr}$
N_{Pr} = $C_p\mu/k$
N_{Re} = Reynolds number, $2Du_b\rho/\mu$
N_{Reo} = $Du_b\rho/\mu$
N_{Rew} = Dv_w/ν
N_{Sto} = Stanton number, $\rho C_p v_w/h_o$

Subscripts

b = average
m = maximum
w = wall
l = lower wall

LITERATURE CITED

1. Eckert, E. R. G., A. J. Diaguila, and P. L. Donoughe *Natl. Advisory Comm. Aeronaut. Tech. Note* 3339 (1955).
2. ———, and R. M. Drake, "Heat and Mass Transfer," McGraw-Hill, New York (1959).
3. Gill, W. N., and M. Scher, *A.I.Ch.E. Journal*, 7, 61 (1961).
4. ———, and S. M. Lee, *ibid*, 8, 303 (1962).
5. Mickley, H. S., R. C. Ross, A. L. Squyers, and W. E. Stewart, *Natl. Advisory Comm. Aeronaut. Tech. Note 3208* (1954).
6. Yuan, S. W., *J. Math. Phys.*, 38, 166 (1959).
7. ———, and A. B. Finkelstein, "Heat Transfer and Mechanics Institute," Stanford Univ., Stanford, California (1956).
8. ———, R. F. Pohler, and W. F. Walker, *Developments in Mechanics*, 1, 526 (1961).

ACKNOWLEDGMENT

This work was sponsored in part by the Office of Naval Research under Contract NONR-669(17). The authors also are indebted to the Syracuse University Computing Center for the use of its facilities.

Manuscript received March 2, 1964; revision received May 22, 1964; paper accepted June 2, 1964.

APPENDIX

The values of S_j ($j = 1, 2, \ldots, 6$) used in Equations (7*a*) and (7*b*) are given by

$$S_1 = \int_o^1 \frac{U}{\left(\frac{1}{N_{Reo}} + L_m^2 \left|\frac{dU}{d\eta}\right|\right)} d\eta$$

$$S_2 = \int_o^1 \frac{\eta}{\left(\frac{1}{N_{Reo}} + L_m^2 \left|\frac{dU}{d\eta}\right|\right)} d\eta$$

$$S_3 = \int_o^1 \frac{1}{\left(\frac{1}{N_{Reo}} + L_m^2 \left|\frac{dU}{d\eta}\right|\right)} d\eta$$

$$S_4 = \int_o^1 \frac{(1-\eta)\,U}{\left(\frac{1}{N_{Reo}} + L_m^2 \left|\frac{dU}{d\eta}\right|\right)} d\eta$$

$$S_5 = \int_o^1 \frac{(1-\eta)\,\eta}{\left(\frac{1}{N_{Reo}} + L_m^2 \left|\frac{dU}{d\eta}\right|\right)} d\eta$$

$$S_6 = \int_o^1 \frac{(1-\eta)}{\left(\frac{1}{N_{Reo}} + L_m^2 \left|\frac{dU}{d\eta}\right|\right)} d\eta$$

The expression for the bulk mean temperature θ_b is

$$\theta_b = \frac{4N_{Rew}}{Q_6^2}\left\{\left(\frac{Q_2}{2} - \frac{Q_4}{3} + Q_3\right) + (e^{N_{Rew}} - 1)\left[\frac{Q_3}{2} + \frac{Q_2}{3} - \frac{Q_4}{4} - \frac{(Q_5 + Q_3)}{N_{Rew}}\right] + \frac{Q_5}{2N_{Rew}}(e^{2N_{Rew}} - 1) + \frac{Q_1}{N_{Rew}N_{Pr}}(e^{N_{Rew}N_{Pr}} - 1) - [e^{N_{Rew}}(N_{Rew} - 1) + 1]\left[\frac{Q_5\,(e^{N_{Rew}} - 1)}{N_{Rew}^2} + \frac{Q_2}{N_{Rew}^2} + \frac{2Q_4}{N_{Rew}^3}\right] + [e^{N_{Rew}N_{Pr}}(N_{Rew}N_{Pr} - 1) + 1]\frac{Q_1\,(e^{N_{Rew}} - 1)}{N_{Rew}^2 N_{Pr}^2} + \frac{Q_4\,e^{N_{Rew}}}{N_{Rew}} - \frac{Q_1(e^{N_{Rew}(1+N_{Pr})} - 1)}{N_{Rew}(1 + N_{Pr})}\right\}$$

$$-\frac{2\left(\frac{d\theta}{d\eta}\right)_o}{N_{Pr}\,Q_6}\left\{1-\frac{(e^{N_{Rew}N_{Pr}}-1)}{N_{Pr}N_{Rew}}+(e^{N_{Rew}}-1)\left(\frac{1}{2}-\frac{1}{N_{Rew}}\right)-\frac{(e^{N_{Rew}}-1)}{N^2_{Pr}N^2_{Rew}}\right.$$

$$\left.[e^{N_{Rew}N_{Pr}}(N_{Rew}N_{Pr}-1)+1]+\frac{(e^{N_{Rew}(1+N_{Pr})}-1)}{N_{Rew}(1+N_{Pr})}\right\}$$

and the values of Q_n $(n = 1, \ldots, 6)$ are given by

$$Q_1=\frac{1}{N_{Rew}N^2_{Pr}}+\frac{(e^{N_{Rew}}-1)}{N^2_{Rew}N^3_{Pr}}+\frac{1}{N_{Rew}(1-N_{Pr})}+\frac{1}{N_{Rew}N_{Pr}}$$

$$Q_2=-\left(\frac{1}{N_{Pr}}+\frac{(e^{N_{Rew}}-1)}{N_{Rew}N^2_{Pr}}\right)$$

$$Q_3=-\left(\frac{1}{N_{Rew}N^2_{Pr}}+\frac{e^{N_{Rew}}-1}{N^2_{Rew}N^3_{Pr}}+\frac{1}{N_{Rew}N_{Pr}}\right)$$

$$Q_4=\frac{e^{N_{Rew}}-1}{2N_{Pr}}$$

$$Q_5=\frac{1}{N_{Rew}(1-N_{Pr})}$$

$$Q_6=(N_{Rew}+2)+e^{N_{Rew}}(N_{Rew}-2)$$

Vapor Phase Activity Coefficients and Standard State Hypothetical Vapor Fugacities for Hydrocarbons

DWIGHT S. HOFFMAN, J. REED WELKER, V. N. P. RAO, and JAMES H. WEBER

University of Idaho, Moscow, Idaho

In an earlier paper Hoffman et al. (*1*) discussed a method for predicting the vaporization equilibrium ratios, defined as y/x, for the components of a multicomponent mixture through use of standard state liquid fugacities, standard state vapor fugacities, liquid phase activity coefficients, and vapor phase activity coefficients. As used here and throughout this paper, standard state fugacity means the fugacity of a pure component at the temperature and pressure of the system. The relationship among these variables has been shown to be

$$K_i'=\frac{\gamma_i^{\,L}}{\gamma_i^{\,v}}\frac{1}{Z_i}\frac{P_{v_i}}{P} \tag{1}$$

where

$$\gamma_i^{\,L}=\frac{(f_i)_L}{(f_i^{\circ})_L\,x_i} \tag{2}$$

$$\gamma_i^{\,v}=\frac{(f_i)_v}{(f_i^{\circ})_v\,y_i} \tag{3}$$

and

James H. Weber is at the University of Nebraska, Lincoln, Nebraska. J. Reed Welker is with the Oil Recovery Corporation, Norman, Oklahoma.

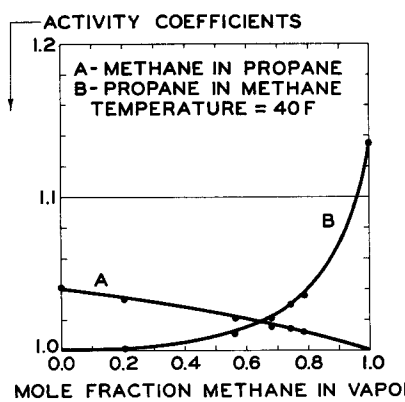

Fig. 1. Vapor phase activity coefficients in the methane-propane system.

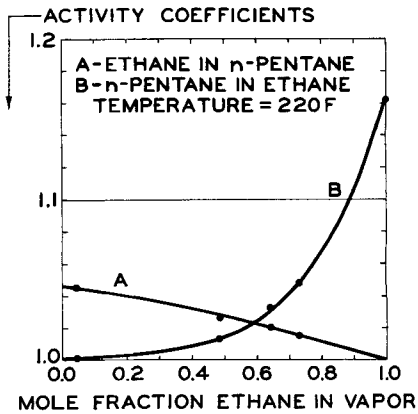

Fig. 2. Vapor phase activity coefficients in the ethane-*n*-pentane system.